e-ISSN 2083–4640
ISSN 1507–1367

RESEARCH PAPER

Reports of Practical Oncology and Radiotherapy
2022, Volume 27, Number 5, pages: 821–831
DOI: 10.5603/RPOR.a2022.0098
Submitted: 23.06.2022
Accepted: 01.08.2022

# Effects of metal implants and validation of four treatment planning methods used for radiotherapy dose calculation

Amirtharaj Gnanasambandam[1, 2], N. Arunai Nambi Raj[2], Sollinselvan K[1]

[1]Department of Radiation Oncology, MIOT Hospitals, Manapakkam, Chennai, India
[2]School of Advanced Sciences, Vellore Institute of Technology, Vellore, India

## ABSTRACT

**Background:** The radiotherapy treatment planning process involves target delineation and dose calculation, both of which directly depend on image quality and Hounsfield unit (HU) accuracy of computed tomography (CT) images. CT images of patients having metal implants undergo image quality deterioration and show inaccurate HU values due to various artifacts. Metal artifact reduction (MAR) is used to improve the image quality. In this study, four treatment planning methods with and without MAR, in combination with actual and assigned HU values, were analyzed for dose calculation accuracy. The aim was to study the effects of metal implants on planning CT and to evaluate the dose calculation accuracy of four treatment planning methods for radiotherapy.

**Materials and methods:** Two phantoms with six different metal inserts were scanned in the extended HU mode, with and without MAR. Geometry verification and HU analysis of the metals and the surrounding region were carried out. Water equivalent distance (WED) measurements and dose calculation for each metal insert were done in the treatment planning system (TPS) using the anisotropic analytical algorithm (AAA). Point dose and two-dimensional dose distribution were studied. Percentage variation analysis between calculated and measured doses and gamma evaluation were conducted to determine the most suitable method for treatment planning.

**Conclusion:** This study concludes that an MARCT image with an assigned HU similar to that of the metal implant is better for contouring and high dose calculation accuracy. If MAR is not available, the actual HU value from the extended HU CT for the metal should be used for dose calculation.

**Key words:** metal implant; metal artifact reduction; extended Hounsfield unit; dose calculation; treatment planning

*Rep Pract Oncol Radiother 2022;27(5):821–831*

## Introduction

The role of radiotherapy in the treatment for various cancers is well known. Accuracy of the radiation dose delivered to patients is critical to exploit the therapeutic window of dose response curves. The International Commission on Radiation Units and Measurements (ICRU) recommends an absorbed dose accuracy of 5% or a distance to agreement (DTA) of 5 mm to 85% of target volume samples in low and high dose gradient regions, respectively [1]. Estimated overall cumulative uncertainty of the delivered dose is 1.9–3.4% under normal conditions, and with lung involvement, it increases up to 5.2% [2]. In addition, the presence of implant materials in patients increases dose uncertainty.

**Address for correspondence:** Arunai Nambi Raj, PhD, School of Advanced Sciences, Vellore Institute of Technology, Vellore — 632014, India; e-mail: narunainambiraj@vit.ac.in

In treatment planning, CT images play a key role in target delineation, dose calculation, and patient setup verification. CT image quality and HU accuracy directly influence the treatment planning process. CT images of patients having metal implants such as dental filling, spinal fixture, hip prosthesis, and mesh show significant deterioration in image quality and inaccurate HU values due to artifacts. This may be due to artifacts caused by beam hardening, scatter, and noise [3, 4]. In a CT image, metals show up as white and dark streaks along the axis of the greatest attenuation, which are caused by the combination of beam hardening and scatter [5]. Furthermore, photon starvation due to strong attenuation results in statistical errors, which are present in CT images as thin dark and bright streaks surrounding the metal implant. These artifacts and HU saturation lead to inaccurate estimation of HU values and, consequently, inaccurate relative electron density (RED) values which are used for dose calculation in the treatment planning system (TPS). CT images with artifacts are challenging for target and normal structure contouring, and inaccurate HU values affect the dose calculation accuracy.

Conventionally, treatment planning with a known implant material is carried out by contouring the artifact regions and the implant to assign appropriate HU values. If implant details, such as dimensions and composition, are not known or not traceable, contouring and assigning HU values become uncertain. With the introduction of the extended HU mode, HU saturation can be avoided and the dose can be calculated without assigning the HU [6]. Metal artifact reduction (MAR) methods, which are used to mitigate artifacts, have become available commercially. CT scans with the MAR method (MARCT) has been assessed for its applicability in treatment planning by many authors [7–13]. In addition, restoration of HU values using MAR and dosimetric differences between MARCT and CT scans without using MAR (WOMARCT) images have also been studied. Whereas a few studies have used the density override method, some have carried out dose calculation with the HU value given by the CT scanner, that is without any manual HU assignment or density override to metal inserts (actual HU).

The mixed availability of MAR and extended HU modes and the change in HU from the center to the periphery of the metal prompted us to study various planning methods for dose calculation, as follows:

- MARCT with actual HU (MAR-ACT);
- WOMARCT with actual HU (WOMAR-ACT);
- MARCT with assigned HU (MAR-ASGN);
- WOMARCT with assigned HU (WOMAR-ASGN).

The dose prediction accuracy of these four planning methods was compared.

For the purpose of this study, two phantoms were constructed with different low and high density metal inserts of known dimensions and density. With the extended HU mode, MARCT and WOMARCT scans of these phantoms were taken. They were then studied to investigate the geometry and HU values inside the metals and in the surrounding regions of the phantom, followed by estimation of dose calculation accuracy. Changes in water equivalent distance (WED) were noted. Point doses were measured below the inserts and were compared with the calculated values for all four methods. Two-dimensional (2D) planar dose distributions were analyzed using the gamma evaluation technique.

## Materials and methods

### Phantoms

A phantom was prepared with inserts of aluminum, titanium, stainless steel, cerrobend, amalgam, and gold of density 2.69, 4.44, 7.77, 9.40, 15.00, and 19.32 g/cm$^3$, respectively, and was labeled HD1. All the inserts were cylindrical with diameter 1 cm ± 0.4 mm and height 2 cm ± 2 mm, except for amalgam and gold. The diameter and height of the amalgam insert were 0.5 cm ± 0.3 mm and 2 cm ± 2 mm, respectively. The gold insert was a stud with diameter 0.14 cm and height 1 cm with a pin head. The inserts were placed sequentially, separated by acrylic rods of length 2 cm ± 2 mm and diameter 1 cm ± 1 mm. This arrangement was maintained along the in-plane axis of two acrylic plates of dimensions 30 × 30 cm$^2$ and thickness 1 cm each, with a slot at their center to accommodate the inserts. This acrylic plate assembly was sandwiched between polymethylmethacrylate (PMMA) plates

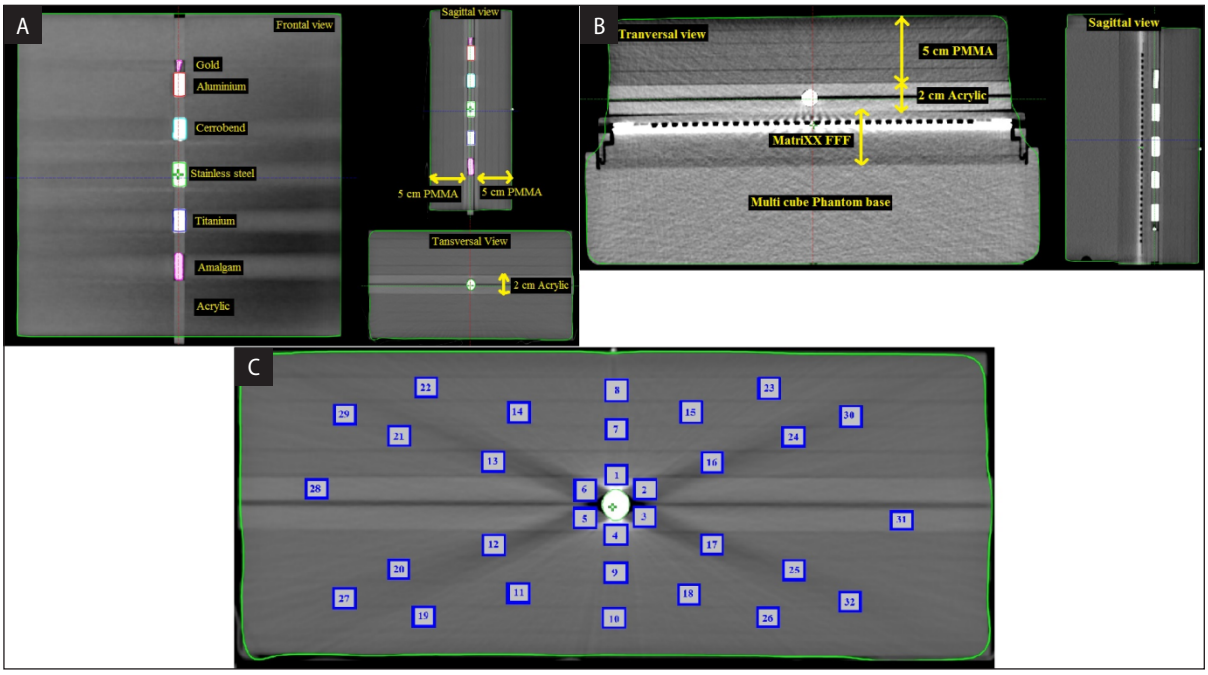


**Figure 1. A.** Computed tomography (CT) image of Phantom HD1; **B.** CT image of Phantom HD2; **C.** Region of interest (ROI) positions for Hounsfield unit (HU) analysis

of 5cm to constitute phantom HD1, as shown in Figure 1A. The PMMA plate below the acrylic plate assembly was replaced with an adapter plate to accommodate a CC13 chamber for point dose measurements.

The acrylic plate assembly was then placed over MatriXX$^{FFF}$ (IBA Dosimetry, Germany), with the lower part of the multicube phantom, to constitute phantom HD2 (Fig. 1B). These phantoms were scanned using Discovery CT750 HD (GE Healthcare, USA) with fiducial markers to reproduce the setup during measurement. With the extended HU mode, scans were acquired with and without MAR. Tube voltage 120 kV, current 250 mAs, field of view 50 cm, and slice thickness 1.25 mm were chosen.

## Geometry verification

Dimensions of the inserts were measured physically and also verified using planar X-ray images of the phantoms. We measured the diameters of the inserts using full-width half maximum (FWHM) from the HU profile. Volume and diameter of each cylindrical metal insert were also calculated. Height of the cylinders was maintained as measured physically to avoid slice interpolation being included as volume change. As the gold insert was non-cylindrical and small, its diameter was measured directly from the image.

## HU Analysis

All the metal inserts were contoured to determine HU values. Descriptive statistics methods mean and standard deviation (SD) were used in this study. Minimum, maximum, mean, and SD of HU values were determined for MARCT and WOMARCT. To investigate the HU variation surrounding the metals, 32 regions of interest (ROI) of dimensions 5 mm × 5 mm were created in the CT images around different inserts and labeled as shown in Figure 1C. Mean HU values at the level of each insert were observed at all 32 positions in both image sets. The influence of the metal on the surrounding region of the phantom was evaluated by finding the difference in HU values between corresponding positions on MARCT and WOMARCT images at different metal insert levels, and these values were compared with those of the acrylic insert level (reference). In addition, any HU difference above 40 HU was identified in color wash, as discussed by Kilby et al. [14] HU profiles along the radial axis were evaluated to analyze changes in HU values from the periphery of the metal to its center.

### WED measurement

Eclipse™ TPS version 13.7 (Varian Medical Systems, Inc.) was used for WED measurements. WED was calculated using TPS with an electron density associated with the respective HU value in the image [15]. For all the four methods, changes in the beam path length were quantified. The beam path length is the distance from the surface of phantom HD1 at the entry point of the field to the ion chamber center, passing through the metal insert, and it was calculated for all inserts.

### Point dose verification

Treatment plans were created using Eclipse™ TPS with a single AP field placed over the center of each insert, including an acrylic insert. Plans were calculated for fixed 50 MU for photon energies 6, 10, 15, 6, and 10 FFF, with field size 5 × 5 $cm^2$, just covering the single insert for that plan. As using multiple beams from different angles can dilute the dosimetric effects, we restricted our study to a single AP field. The CC13 thimble chamber's active volume of 1.3 $cm^3$ was contoured below the inserts. Dose calculation was done using AAA algorithm. The existing HU to RED CT calibration curve was extended to high-density metals. Mean dose values at the contoured chamber's active volume were determined for different energies and inserts using MAR-ACT, WOMAR-ACT, MAR-ASGN, and WOMAR-ASGN for all photon energies. The plan setup was reproduced and delivered in Truebeam STx linear accelerator (Varian Medical Systems, Palo Alto), and the doses were measured using CC13 chamber and Dose1 electrometer (IBA Dosimetry). Percentage variation between the calculated dose and the measured dose under different metals for different energies was also calculated.

### 2D planar dose verification

Phantom HD2 was used for planar dose verification of all four planning methods. A plan with a single AP field of field size 10 × 24 $cm^2$ was created to cover all the inserts simultaneously, and plans to cover each of the inserts individually with a field size of 6 × 6 $cm^2$ were created and measured using 2D ion chamber array MatriXX$^{FFF}$ (IBA Dosimetry). Gamma evaluation of the measured dose against the calculated dose was performed using dose difference (DD), DTA criteria of (3 %, 3 mm) and (2 %, 2 mm), and the results were noted. Gamma analysis results of the calculated dose distribution of MARCT were compared with those of WOMARCT at sagittal and frontal planes.

### Combined ranking

To summarize the effects, arbitrary ranking method was used, as shown in Table 1. Synergetic ranking was performed to identify the most suitable treatment planning method in all aspects by adding the ranks obtained.

## Results and Discussion

### Geometry verification

Metal inserts in WOMARCT images showed shape distortion and radial volume growth. In MARCT images, the metal inserts maintained their shape but showed radial volume growth. Jessie Y Huang et al. found that a stainless steel insert of diameter 2.86 cm and a titanium insert of diameter 0.95 cm were underestimated by −0.14 cm and −0.26 cm, respectively; in their MARCT images [16]. Vicky W. Huang reported that a stainless steel insert of diameter 1.9 cm was overpredicted by 0.09 cm [17].

In our study, using the FWHM method to estimate the diameter, the variation in MARCT was measured to be −0.11 to 0.02 cm, and in WOMARCT, it was −0.01 to 0.03 cm. The WOMARCT FWHM method showed better agreement with physical measurements of diameter for all the metal inserts. In the contouring method, MARCT showed a difference of 0.16 cm for stainless steel, cerrobend,

**Table 1.** Ranking method

| Point dose | WED [cm] | Gamma passing area (2 mm; 2%) | Artifact | Score |
|---|---|---|---|---|
| 0–2% | 0–0.1 | 90–100% | Absence | 1 |
| 2–5% | 0.1–0.5 | 80–90 % | – | 2 |
| 5–10% | 0.5–1 | 70–80% | Presence | 3 |
| > 10% | > 1 | < 70% | – | 4 |

WED — water equivalent distance

**Table 2.** Geometry verification of metal inserts

| Metal | Physical diameter [cm] | MAR diameter [cm] | | WOMAR diameter [cm] | |
|---|---|---|---|---|---|
| | | Contoured | FWHM | Contoured | FWHM |
| Aluminum | 0.96 | 1.00 | 0.98 | 1.00 | 0.98 |
| Titanium | 0.98 | 1.06 | 0.89 | 1.12 | 0.99 |
| Stainless steel | 0.98 | 1.14 | 0.92 | 1.14 | 0.99 |
| Cerrobend | 0.98 | 1.14 | 0.91 | 1.16 | 0.99 |
| Amalgam | 0.53 | 0.70 | 0.42 | 0.78 | 0.56 |
| Gold | 0.14 | 0.30 | 0.16 | 0.32 | 0.13 |

MAR — metal artifact reduction; WOMAR — without metal artifact reduction; FWHM — full-width half maximum

and gold inserts and 0.17 cm for the amalgam insert. WOMARCT showed a difference of 0.14, 0.16, 0.18, 0.25, and 0.18 cm for titanium, stainless steel, cerrobend, amalgam, and gold inserts, respectively (Tab. 2). Both MARCT and WOMARCT in the contouring method overpredicted the diameter.

An increase of 2 mm in thickness in a stainless steel insert with a density of 8 g/cm$^3$ can introduce a water equivalency thickness of 1.6 cm. If actual dimensions are known and volume growth is significant, we recommend that contouring the actual size of the implant and assigning the appropriate HU value have to be performed first, followed by contouring the excess volume growth and assigning the surrounding tissue's HU value.

## HU Analysis

### HU value of metal inserts

HU values of metals measured with the standard square ROI cannot include all the values of different shape metals. Moreover, single-point measurements are highly susceptible to noise. Contouring the whole metal inserts includes all values to find the mean HU value. However, the change in the HU value from edges to the center makes finding the representative value of a particular metal challenging. As HU values depend on various parameters such as tube voltage, field of view, patient thickness, metal insert's density and size, and MAR, a single HU to RED CT calibration curve does not suffice for conditions that are not calibrated references [18]. Mean HU values measured in our study for the metals were not proportional to their density (Tab. 3). For known metals, HU values can be assigned to reflect their respective RED. Maximum HU values were higher in MARCT for all inserts compared with those of WOMARCT, except for amalgam and gold. The mean HU values were lower and SD values were high in MARCT.

### HU analysis of insert surroundings

The average of absolute difference between WOMARCT and MARCT in mean HU values at different metal inserts compared with that of the acrylic level in the immediate vicinity at ROI 1 to 6 was determined as follows: aluminum 36–36; titanium 140–27; stainless steel 300–32; cerrobend 452–44; amalgam337–25; and gold 46–16. ROI 12, 13, 16, and 17 at the inner circle next to the center ROI and ROI 20, 21, 24, and 25 at the outer circle, which fell under the streak artifacts in WOMARCT,

**Table 3.** Hounsfield unit (HU) value of metal inserts

| Metal insert | MARCT | | | | WOMARCT | | | |
|---|---|---|---|---|---|---|---|---|
| | HU min. | HU max. | HU mean | SD | HU min. | HU max. | HU mean | SD |
| Aluminum | 237 | 2235 | 1517 | 666 | 382 | 2243 | 1674 | 594 |
| Titanium | –78 | 9559 | 5771 | 3137 | 1142 | 8788 | 6462 | 2247 |
| Stainless steel | –113 | 17108 | 9021 | 5361 | 1170 | 16539 | 10515 | 4605 |
| Cerrobend | –452 | 26241 | 10413 | 6835 | 247 | 23379 | 12080 | 6202 |
| Amalgam | –471 | 29441 | 8875 | 9397 | 297 | 30985 | 14140 | 10211 |
| Gold | –691 | 31046 | 4342 | 6147 | –1000 | 31743 | 5346 | 8104 |

MARCT — computed tomography with metal artifact reduction; WOMARCT — computed tomography without metal artifact reduction; SD — standard deviation

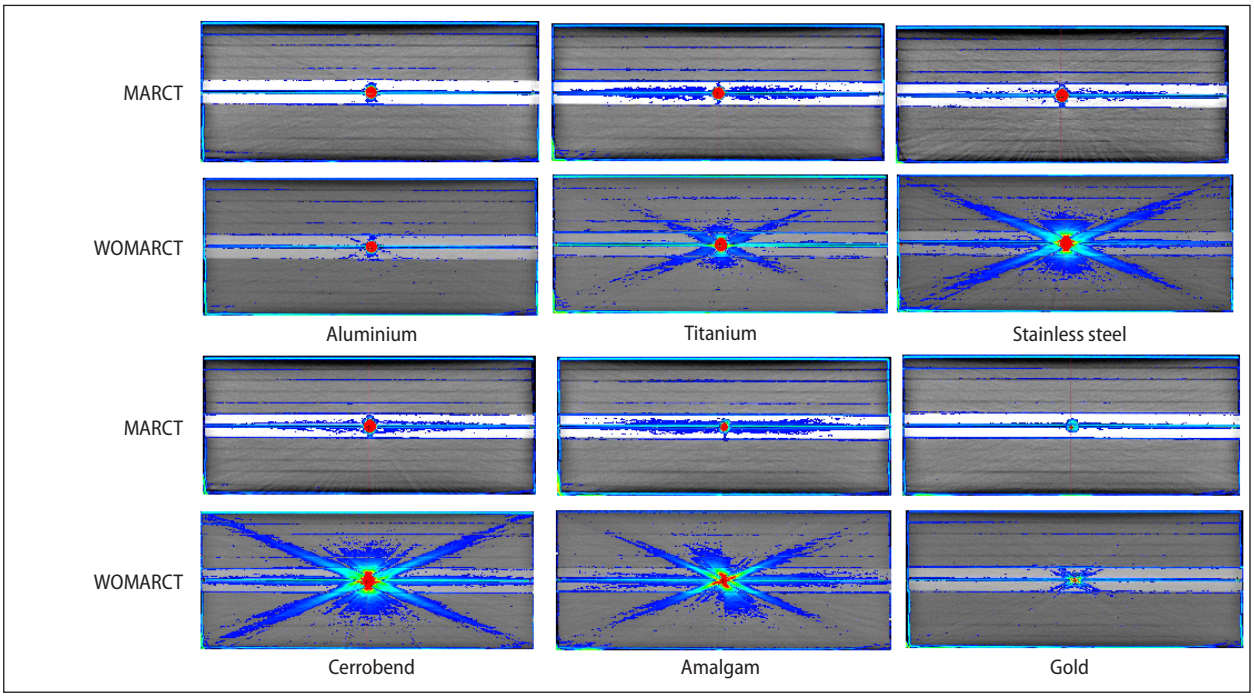


**Figure 2.** Image difference color wash. MARCT — computed tomography with metal artifact reduction; WOMARCT — computed tomography without metal artifact reduction

showed the average of absolute difference of 7, 32, 69, 88, 51, and 5 for aluminum, titanium, stainless steel, cerrobend, amalgam, and gold, respectively. The remaining ROI at WOMARCT showed an average of 11. In MARCT, except ROI 1 to 6, the remaining ROI had an average difference of 4.

ROI 1, 4, 7, and 9 were at the region of bright artifacts on the lowest attenuation path and were influenced by high-density metals in both image sets. MAR controlled the impact on HU values in the surrounding area of the metal by eliminating the dark streak artifacts, which fell along the greatest attenuation axis. Guilfoile C et al. and Vicky W. Huang also showed that MAR can restore the HU values successfully [19, 17].

Figure 2 shows the color wash of > 40HU difference in both the image sets for all the metals used. The difference seen horizontally at the level of the insert is due to the air gap in the phantom.

### HU difference from the periphery to the center

A metal with uniform density kept inside the phantom shows up in the images as bright at the edges and dark at the center, which is termed pseudo-cortex effect by Rodney A. Brooks.[20] High-density metals, such as gold and cerrobend, may show even air packets at the core. In our study, MARCT showed a smaller difference in the HU profile than WOMARCT for all the metals (Tab. 4). HU values at the center of cerrobend, stainless steel, and gold observed from the HU profile were the same (≈11500 HU) as shown in Figure 3, which illustrates the depth of this effect.

## WED measurements

WED measurements show the difference in the beam path length due to changes in geometry of metal inserts, artifacts, assigning HU values, and changes in HU values from the center to the periphery. Measured and calculated WED values were in good agreement for acrylic and aluminum in all the methods (< 1 mm). For metals other than these, the differences in increase in WED were as follows: 0.14 ± 0.60 cm, 0.50 ± 0.17 cm, −0.59 ± 0.73 cm, and 1.31 ± 0.52 cm for MAR-ASGN, WOMAR-ACT, MAR-ACT, and WOMAR-ASGN, respectively. Shape distortion and artifacts in WOMARCT led to overcontouring and resulted in higher differences.

## Point dose measurements

All four methods predicted the dose delivered below acrylic, aluminum, and titanium inserts well, and the average percentage deviation over all

**Table 4.** Hounsfield unit (HU) values at periphery and center of metal inserts

| Metal | WOMARCT | | | MARCT | | Difference |
|---|---|---|---|---|---|---|
| | HU periphery | HU center | Difference | HU periphery | HU center | |
| Aluminum | 2121 | 2012 | 109 | 2087 | 1989 | 98 |
| Titanium | 9038 | 7404 | 1634 | 9423 | 8563 | 860 |
| Stainless steel | 17288 | 11487 | 5801 | 16979 | 12880 | 4099 |
| Cerrobend | 25057 | 11640 | 13417 | 23694 | 13063 | 10631 |
| Amalgam | 31241 | 24359 | 6882 | 29962 | 26469 | 3493 |

WOMARCT — computed tomography without metal artifact reduction; MARCT — computed tomography with metal artifact reduction

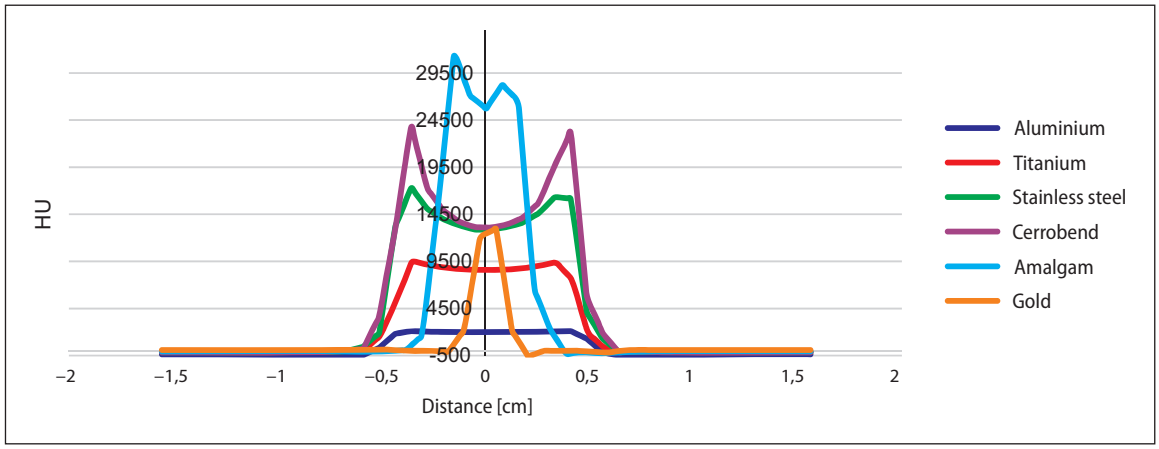


**Figure 3.** Hounsfield unit (HU) profile of different metal inserts (WOMARCT)

photon energies was 0.80 ± 0.71. The average percentage variation for MAR-ACT, WOMAR-ACT, MAR-ASGN, and WOMAR-ASGN methods using high-density metals was as follows: stainless steel 3.99 ± 0.54, −0.61 ± 0.64, 0.61 ± 0.54, and −2.46 ± 1.06; cerrobend 12.87 ± 1.91, 7.29 ± 0.99, 8.11 ± 1.14, and 3.80 ± 1.07; amalgam 1.98 ± 0.81, −3.73 ± 0.77, −2.00 ± 0.45, and −5.23 ± 1.13; and gold 0.59 ± 0.40, −0.15 ± 0.39, −3.11 ± 0.31, and −3.00 ± 0.28, respectively. While doses for low-density metals were well predicted by TPS (< 2.3%), high-density metals starting from stainless steel showed higher deviations, as high as 16.3% (cerrobend–MAR-ACT–6 FFF) (Tab. 5). As amalgam and gold used in this study had smaller diameter, their percentage variations were also smaller, albeit with higher densities. Along with the prediction of attenuation by metals, scatters, artifacts, and beam transport through metals can also lead to changes in accuracy.

MAR-ACT showed higher doses and WOMAR-ASGN showed lower doses at downstream. As shown in Figure 4, MAR-ASGN and WOMAR-ACT showed nearly equal doses and had better agreement with measured doses below the stainless steel insert. Although cerrobend also exhibited this pattern, it showed a higher percentage variation with measured doses and did not correlate with the WED measurements.

In treatment planning, WOMARCT images can be used with actual HU values of the implants, as shape distortion and changes in geometry increase the uncertainty in contouring and assigning the HU value. MARCT can be used with assigned HU values as MAR-ACT has shown a higher percentage variation than MAR-ASGN.

## 2D Dose Distribution Analyses

Gamma evaluation using (DTA: 3mm, DD: 3%) criteria passes 100% area for gamma value < 1 for all the tests carried out. While point dose measurements showed percentage variations up to 16.3% below the cerrobend insert, gamma evaluation was not sensitive enough to detect the same. On stringent evaluation (DTA: 2mm, DD: 2%), the passing area reduced significantly (Tab. 6). MAR-ASGN showed a better passing rate compared with other methods.

**Table 5.** Percentage variation of calculated dose with measured dose

| Metal insert | Energy | Measured dose [cGy] | Percentage variation with measured dose (%) | | | |
|---|---|---|---|---|---|---|
| | | | MAR-ACT | WOMAR-ACT | MAR-ASGN | WOMAR-ASGN |
| Acrylic | 6X | 36.84 | 0.16 | 0.16 | 0.43 | 0.43 |
| | 10X | 40.75 | –0.61 | –0.37 | –0.37 | –0.37 |
| | 15X | 42.56 | 0.09 | 0.33 | 0.33 | 0.33 |
| | 6FFF | 35.31 | –0.03 | 0.25 | 0.54 | 0.54 |
| | 10FFF | 40.46 | –0.40 | –0.15 | –0.15 | 0.10 |
| Aluminium | 6X | 35.35 | 0.99 | 1.27 | 0.71 | 0.42 |
| | 10X | 39.35 | 0.64 | 0.89 | 0.38 | 0.38 |
| | 15X | 41.16 | 1.55 | 1.55 | 1.31 | 1.07 |
| | 6FFF | 33.65 | 1.04 | 1.63 | 0.74 | 0.74 |
| | 10FFF | 38.89 | 1.05 | 1.05 | 0.80 | 0.54 |
| Titanium | 6X | 33.65 | 1.93 | 0.45 | 1.93 | 0.74 |
| | 10X | 37.78 | 1.64 | 0.58 | 1.64 | 0.85 |
| | 15X | 39.69 | 2.29 | 1.28 | 2.29 | 1.54 |
| | 6FFF | 31.85 | 2.04 | 0.47 | 2.04 | 0.78 |
| | 10FFF | 37.21 | 1.59 | 0.51 | 1.85 | 0.78 |
| Stainless steel | 6X | 30.63 | 4.15 | –0.75 | –0.75 | –3.04 |
| | 10X | 35.06 | 3.25 | –0.74 | –0.46 | –2.17 |
| | 15X | 37.05 | 3.91 | 0.40 | 0.67 | –0.94 |
| | 6FFF | 28.69 | 4.22 | –1.36 | –1.01 | –3.80 |
| | 10FFF | 34.21 | 3.77 | –0.61 | –0.32 | –2.37 |
| Cerrobend | 6X | 27.79 | 12.99 | 6.51 | 7.23 | 2.20 |
| | 10X | 32.1 | 11.21 | 6.23 | 6.85 | 3.43 |
| | 15X | 33.98 | 11.83 | 7.42 | 8.00 | 5.06 |
| | 6FFF | 25.29 | 16.25 | 8.74 | 9.53 | 3.99 |
| | 10FFF | 30.87 | 13.05 | 7.55 | 8.20 | 4.31 |
| Amalgam | 6X | 33.02 | 2.36 | –4.60 | –2.48 | –8.54 |
| | 10X | 37.15 | 1.21 | –3.63 | –2.29 | –6.86 |
| | 15X | 39.01 | 1.77 | –2.59 | –1.31 | –5.15 |
| | 6FFF | 30.81 | 3.21 | –4.25 | –1.98 | –8.80 |
| | 10FFF | 36.3 | 1.93 | –3.58 | –1.93 | –7.16 |
| Gold | 6X | 36.37 | 0.36 | –0.19 | –2.94 | –7.07 |
| | 10X | 40.27 | –0.17 | –0.67 | –3.40 | –6.38 |
| | 15X | 42.12 | 0.66 | 0.19 | –2.66 | –5.51 |
| | 6FFF | 34.6 | 0.87 | 0.29 | –3.18 | –7.80 |
| | 10FFF | 39.84 | 0.40 | –0.35 | –3.36 | –6.88 |

MAR-ACT — computed tomography with metal artifact reduction (MARCT) with actual Hounsfield unit (HU); WOMAR-ACT — computed tomography without metal artifact reduction (WOMARCT) with actual HU; MAR-ASGN — MARCT with assigned HU; WOMAR-ASGN — WOMARCT with assigned HU

Sathyathas et al. reported an increase in the gamma passing area with the use of MARCT [21]. Gamma evaluation of frontal and sagittal planes between MARCT and WOMARCT calculated dose distributions passed 100% at (3 mm: 3%) and reduced to 83.4 % at (2 mm: 2%) evaluation. Figure 5 shows

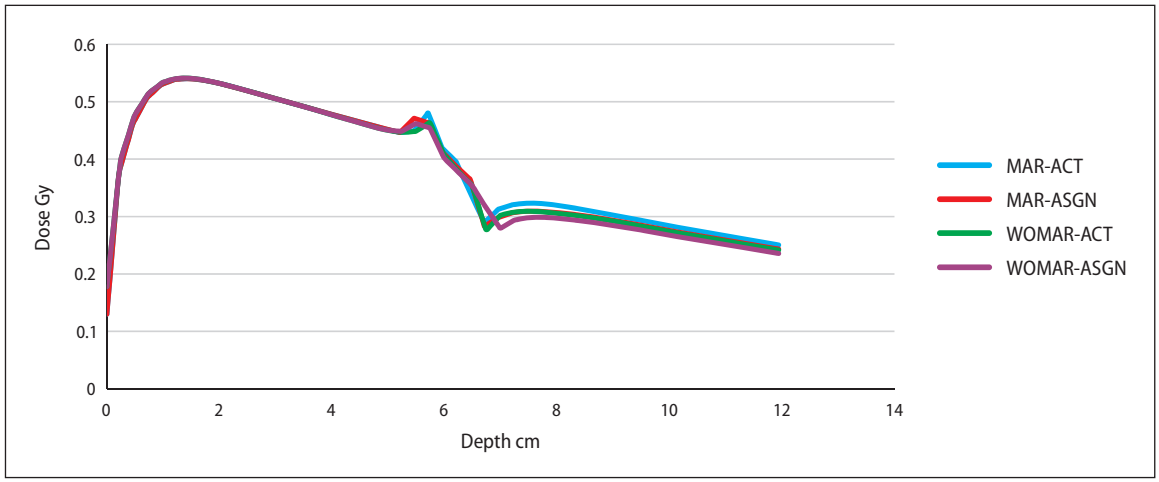


**Figure 4.** Calculated dose profiles at stainless steel level

**Table 6.** Gamma evaluation results

| Metal insert | MAR-ACT DD 2%; DTA 2 mm | WOMAR-ACT DD 2%; DTA 2 mm | MAR-ASGN DD 2%; DTA 2 mm | WOMAR-ASGN DD 2%; DTA 2 mm |
|---|---|---|---|---|
| All | 79.90 | 78.90 | 84.80 | 83.00 |
| Aluminium | 87.60 | 54.10 | 97.80 | 92.50 |
| Titanium | 65.60 | 93.50 | 98.90 | 98.90 |
| Stainless steel | 90.20 | 87.10 | 88.00 | 84.60 |
| Cerrobend | 55.00 | 79.50 | 84.50 | 51.60 |
| Amalgam | 95.70 | 51.70 | 98.80 | 89.40 |

MAR-ACT — computed tomography with metal artifact reduction (MARCT) with actual Hounsfield unit (HU); WOMAR-ACT — computed tomography without metal artifact reduction (WOMARCT) with actual HU; MAR-ASGN — MARCT with assigned HU; WOMAR-ASGN — WOMARCT with assigned HU

the pattern of gamma values around and below the inserts. The influence of metals can be visualized via the gamma pattern. Along with downstream, scatter pattern showed increased gamma values.

## Combined ranking

Addition of ranks according to the accuracy level at different tests was then carried out. Based on the scores obtained (the lower, the better), the tested methods can be arranged as follows: MAR-ASGN, MAR-ACT, WOMAR-ACT, and WOMAR-ASGN with values 32, 42, 45, and 47, respectively.

## Summary

1. Size and shape of the high-density metal have to be estimated correctly in planning CT. If needed, orthogonal planar X- Ray images can be taken for verification.
2. The HU value of the metal depends on various parameters; hence, it has to be assigned to represent its RED. To determine the unknown metal from extended HU CT, standard square ROI or single-point measurements should be avoided. HU should be estimated from clinical experience, contouring, and profile analysis.
3. The extended HU mode in a CT scanner for radiotherapy planning helps to avoid HU saturation.
4. In the absence of MARCT, shape distortion, white streaks, and volume growth can result in the overestimation of the implant size and an increase in the dose discrepancy, if contoured and assigned.
5. MARCT substantially helps to mitigate artifacts around metal implants, but the estimated HU value of the metal does not yield better agreement with the measured one compared with MAR-ASGN.

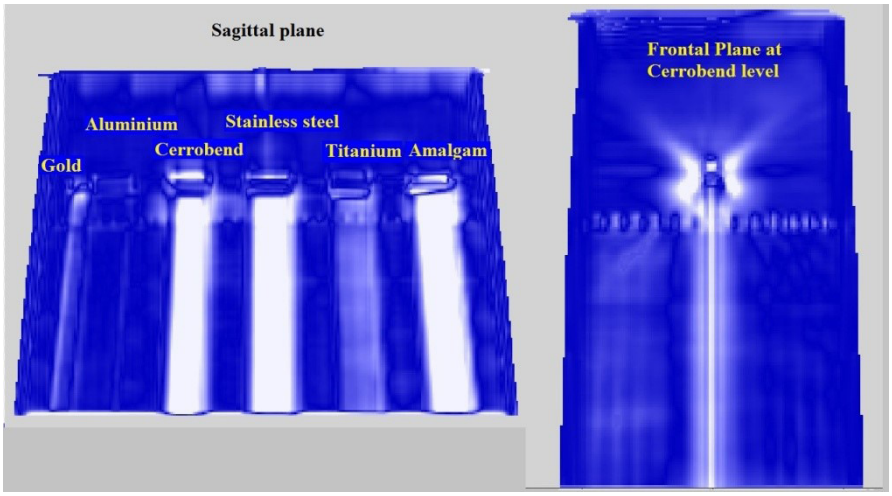


**Figure 5.** Gamma evaluation of computed tomography with metal artifact reduction (MARCT) and computed tomography without metal artifact reduction (WOMARCT) calculated dose distributions

## Conclusion

Geometry of metals in the CT is crucial for dose calculation accuracy. MARCT reduces artifacts around the metal and aids in better delineation of target and normal structures. The planning method preference should be in the order of MAR-ASGN, MAR-ACT, WOMAR-ACT, and WOMAR-ASGN, based on their dose calculation accuracy and artifact reduction.

### Conflicts of interest

The authors have no conflicts of interest to declare.

### Funding

This publication was prepared without any external source of funding.

### Ethical permission

Ethical approval was not necessary for the preparation of this article.

## References

1. Prescribing, Recording, and Reporting Photon-Beam Intensity-Modulated Radiation Therapy (IMRT). J ICRU. 2010; 10(1): Report 83. https://www.icru.org/report/prescribing-recording-and-reporting-intensity-modulated-photon-beam-therapy-imrticru-report-83/.
2. Thwaites D. Accuracy required and achievable in radiotherapy dosimetry: have modern technology and techniques changed our views? J Phys. 2013; Conf Ser(444): 012006.
3. De Man B, Nuyts J, Dupont P, et al. Metal streak artifacts in X-ray computed tomography. IEEE Trans Nucl Sci. 1999; 46: 691–6.
4. Barrett JF, Keat N. Artifacts in CT: recognition and avoidance. Radiographics. 2004; 24(6): 1679–1691, doi: 10.1148/rg.246045065, indexed in Pubmed: 15537976.
5. Drosoula G, et al. Metal artifacts in computed tomography for radiation therapy planning: dosimetric effects and impact of metal artifact reduction. Phys Med Biol. 2017; 62: R49–R80.
6. Mullins JP, Grams MP, Herman MG, et al. Treatment planning for metals using an extended CT number scale. J Appl Clin Med Phys. 2016; 17(6): 179–188, doi: 10.1120/jacmp.v17i6.6153, indexed in Pubmed: 27929492.
7. Ziemann C, Stille M, Cremers F, et al. Improvement of dose calculation in radiation therapy due to metal artifact correction using the augmented likelihood image reconstruction. J Appl Clin Med Phys. 2018; 19(3): 227–233, doi: 10.1002/acm2.12325, indexed in Pubmed: 29664225.
8. Spadea MF, Verburg J, Baroni G, et al. Dosimetric assessment of a novel metal artifact reduction method in CT images. J Appl Clin Med Phys. 2013; 14(1): 4027, doi: 10.1120/jacmp.v14i1.4027, indexed in Pubmed: 23318388.
9. Kratz B, Weyers I, Buzug TM. A fully 3D approach for metal artifact reduction in computed tomography. Med Phys. 2012; 39(11): 7042–7054, doi: 10.1118/1.4762289, indexed in Pubmed: 23127095.
10. Axente M, Paidi A, Von Eyben R, et al. Clinical evaluation of the iterative metal artifact reduction algorithm for CT simulation in radiotherapy. Med Phys. 2015; 42(3): 1170–1183, doi: 10.1118/1.4906245, indexed in Pubmed: 25735272.
11. Li H, Noel C, Chen H, et al. Clinical evaluation of a commercial orthopedic metal artifact reduction tool for CT simulations in radiation therapy. Med Phys. 2012; 39(12): 7507–7517, doi: 10.1118/1.4762814, indexed in Pubmed: 23231300.
12. Shen ZL, Xia P, Klahr P, et al. Dosimetric impact of orthopedic metal artifact reduction (O-MAR) on Spine SBRT patients. J Appl Clin Med Phys. 2015; 16(5): 106–116, doi: 10.1120/jacmp.v16i5.5356, indexed in Pubmed: 26699295.
13. Spadea MF, Verburg JM, Baroni G, et al. The impact of low-Z and high-Z metal implants in IMRT: a Monte Carlo study of dose inaccuracies in commercial dose algorithms.

Med Phys. 2014; 41(1): 011702, doi: 10.1118/1.4829505, indexed in Pubmed: 24387494.
14. Kilby W, Sage J, Rabett V. Tolerance levels for quality assurance of electron density values generated from CT in radiotherapy treatment planning. Phys Med Biol. 2002; 47(9): 1485–1492, doi: 10.1088/0031-9155/47/9/304, indexed in Pubmed: 12043814.
15. Eclipse Photon and Electron reference Guide. 2014;P1008621-001-A, 196-197. Varian Medical Systems.
16. Huang JY, Kerns JR, Nute JL, et al. An evaluation of three commercially available metal artifact reduction methods for CT imaging. Phys Med Biol. 2015; 60(3): 1047–1067, doi: 10.1088/0031-9155/60/3/1047, indexed in Pubmed: 25585685.
17. Huang VW, Kohli K. Evaluation of New Commercially Available Metal Artifact Reduction (MAR) Algorithm on Both Image Quality and Relative Dosimetry for Patients with Hip Prosthesis or Dental Fillings. IJMPCERO. 2017; 6: 124–138.
18. Coolens C, Childs PJ. Calibration of CT Hounsfield units for radiotherapy treatment planning of patients with metallic hip prostheses: the use of the extended CT-scale. Phys Med Biol. 2003; 48: 1591–1603, doi: 10.1088/0031-9155/48/11/308, indexed in Pubmed: 12817940.
19. Guilfoile C, Rampant P, House M. The impact of smart metal artefact reduction algorithm for use in radiotherapy treatment planning. Australas Phys Eng Sci Med. 2017; 40(2): 385–394, doi: 10.1007/s13246-017-0543-5, indexed in Pubmed: 28378320.
20. Brooks RA, Di Chiro G, et al. Beam Hardening in X-Ray Reconstructive Tomography. Phys Med Biol. 1976; 21: 390–398, doi: 10.1088/0031-9155/21/3/004, indexed in Pubmed: 778862.
21. Puvanasunthararajah S, Fontanarosa D, Wille ML, et al. The application of metal artifact reduction methods oncomputed tomography scans for radiotherapy applications: A literature review. J Appl Clin Med Phys. 2021; 22(6): 198–223, doi: 10.1002/acm2.13255, indexed in Pubmed: 33938608.